



University of **HUDDERSFIELD**

University of Huddersfield Repository

Tesfa, Belachew, Horler, Greg, Al Thobiani, Faisal, Gu, Fengshou and Ball, Andrew

A clamping force measurement system for monitoring the condition of bolted joints on railway track joints and points

Original Citation

Tesfa, Belachew, Horler, Greg, Al Thobiani, Faisal, Gu, Fengshou and Ball, Andrew (2012) A clamping force measurement system for monitoring the condition of bolted joints on railway track joints and points. *Journal of Physics: Conference Series*, 364. 012021. ISSN 1742-6596

This version is available at <https://eprints.hud.ac.uk/id/eprint/14138/>

The University Repository is a digital collection of the research output of the University, available on Open Access. Copyright and Moral Rights for the items on this site are retained by the individual author and/or other copyright owners. Users may access full items free of charge; copies of full text items generally can be reproduced, displayed or performed and given to third parties in any format or medium for personal research or study, educational or not-for-profit purposes without prior permission or charge, provided:

- The authors, title and full bibliographic details is credited in any copy;
- A hyperlink and/or URL is included for the original metadata page; and
- The content is not changed in any way.

For more information, including our policy and submission procedure, please contact the Repository Team at: E.mailbox@hud.ac.uk.

<http://eprints.hud.ac.uk/>

A clamping force measurement system for monitoring the condition of bolted joints on railway track joints and points

B Tesfa¹, G Horler, F Al Thobiani, F Gu and A D Ball

School of Computing and Engineering, University of Huddersfield, Queensgate,
HD1 3DH, UK

Email: b.c.tesfa@hud.ac.uk

Abstract: Many industrial structures associated with railway infrastructures rely on a large number of bolted joint connections to ensure safe and reliable operation of the track and trackside furniture. Significant sums of money are spent annually to repair the damage caused by bolt failures and to maintain the integrity of bolted structures. In the U.K., Network Rail (the organization responsible for rail network maintenance and safety) conducts corrective and preventive maintenance manually on 26,000 sets of points (each having approximately 30 bolted joints per set), in order to ensure operational success and safety for the travelling public. Such manual maintenance is costly, disruptive, unreliable and prone to human error. The aim of this work is to provide a means of automatically measuring the clamping force of each individual bolted joint, by means of an instrumented washer. This paper describes the development of a sensor means to be used in the washer, which satisfies the following criteria.

1. Sense changes in the clamping force of the joint and report this fact.
2. Provide compatibility with the large dynamic range of clamping force.
3. Satisfy the limitations in terms of physical size.
4. Provide the means to electronically interface with the washer.
5. Provide a means of powering the washer in situ.
6. Provide a solution at an acceptable cost.

Specifically the paper focuses on requirements 1, 2 and 3 and presents the results that support further development of the proposed design and the realization of a pre-prototype system.

In the paper, various options for the force sensing element (strain gage, capacitor, piezo-resistive) have been compared, using design optimization techniques. As a result of the evaluation, piezo-resistive sensors in concert with a proprietary force attenuation method, have been found to offer the best performance and cost trade-off. The performance of the novel clamping force sensor has been evaluated experimentally and the results show that a smart washer can be developed to monitor the condition of bolted joints as found on railway track and points.

Key words: bolt joint, strain gage sensor, capacitor force sensor, piezo-resistive sensor, elastomer, clamping force, smart washer

¹ To whom any correspondence should be addressed

1. Introduction

According to 2010 statistics, in the U.K. alone there are 40,000km railway track, 2,500 stations and 400 passenger trains that serve more than 1.32 billion passengers [1]. The track on which the train runs is comprised of parallel rails separated and secured by sleepers. The rails are usually bolted or spring loaded to the sleeper with lengths of rail jointed by bolts.

To allow changes in direction, the track has crossings or points, at appropriate locations; these points are complex systems that utilise bolts to connect the various components. Since the greatest concentration of bolts occur in the vicinity of points, it is unsurprising that the majority of accidents and derailments occurring in recent years [2] has been caused by point failure as a result of inappropriately tensioned bolts or missing nuts. Figure 1 illustrates a track with stretcher bars connected by bolts to the track. It also shows a typical bolted joint, comprising a bolt, nut, washer, and two members to be clamped. The purpose of the washer is to provide a smooth load-bearing surface and to prevent damage to a surface of clamping member.

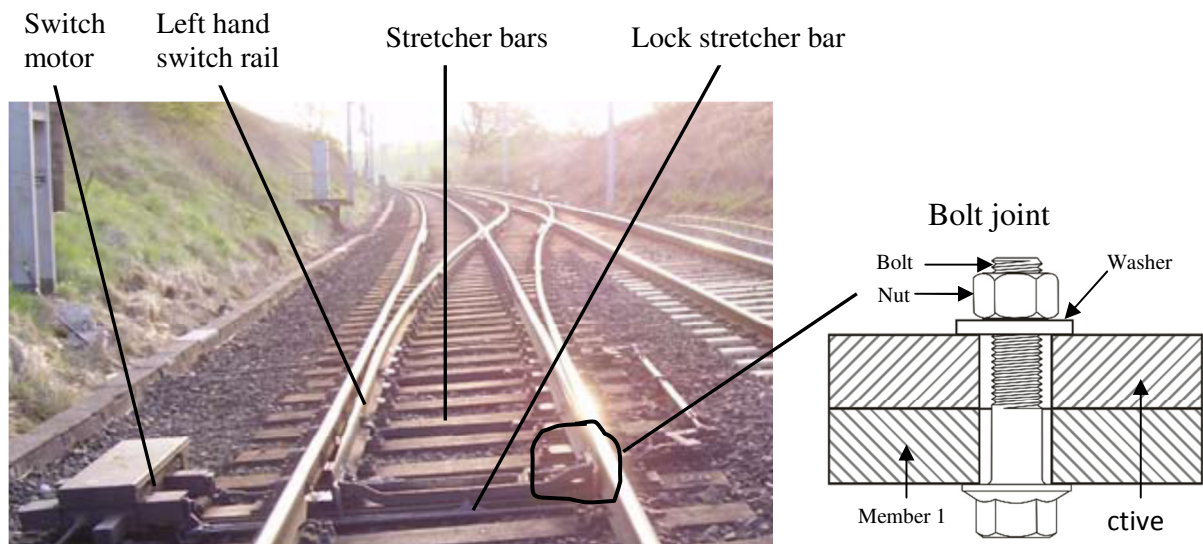


Figure 1. Rail network connection points and a typical bolted joint system [2].

The bolted joints on railway tracks are subject to vibration, varying loads, and other operation parameters that can cause them to be fail; failure mechanisms include material failure, fastener loosening and joint separation. Millions of pounds are spent each year surveying, maintaining and repairing bolt fastenings [3] and the companies and bodies conducting and policing such activities are keen to adopt methods which could improve the reliability of the fastener, safety of the traveling public and reduce the cost in achieving these aims.

The mechanics of the bolt assembly process and bolt behavior during service is complicated and unpredictable. Data from maintenance reports and trackside surveys show that the most common causes of bolted joint failure are metallurgical fatigue, under-tightening, over-tightening and irregular tightening [4]. Any bolted joint that is tensioned incorrectly can degrade the behavior and life of a joint in service and can lead to the joint problems and failure mechanisms mentioned above. As a result, the only method of guaranteeing bolted joint performance is to measure the clamping force directly, as applied by the nut and bolt. Indeed, the use of torque as an indicator of clamping force is far from ideal, as is the assumption that a bolted joint tensioned with a high clamping force will not slacken over time. Thus, it is critically important to monitor bolt tension (clamping force) periodically throughout life of bolted joint.

The current method of inspection involves a visual observation of the joint components and periodic re-torquing of the nut or bolt. While modern digital photography can be used to provide a

visual record of the inspection and state of the joint, there is currently no technology which can provide a measurement of clamping force and a means to uniquely link the clamping force data with each individual joint.

The aim of the project is to identify an appropriate sensor technology, which can withstand the operational rigours associated with the bolted joints as used on points etc. This is a challenge, due to the need for the sensor to be able to withstand and measure high clamping forces (70kN). Furthermore the sensor must be able to respond to small changes in clamping force, which could be indicative of joint failure. In order to achieve these aims it was necessary to undertake a program of design and experimentation so that the most appropriate technological solution could be identified and tested.

2. Clamping force technology

The current method for setting clamping force is by fastening a nut and bolt to a specific torque. This method is unreliable due to:

- At best clamping force is proportional to torque.
- Issues with the thread, such as disfigurement, dirt and corrosion can lead to high torque figures but incorrect (low) clamping forces in the joint.
- Setting the correct torque requires the nut or bolt to be slackened and re-torqued.
- Setting a correct torque requires that the torque wrench is calibrated.
- Labour intensive
- Prone to human error
- The technique of re-torquing is open loop, being neither corrective nor preventative since no measure of clamping force is taken prior to re-torquing.

The preferred method of ensuring joint fastening is to measure the clamping force (bolt tension) directly using automatic methods. In order to do this an appropriate sensor and mechanical arrangement is necessary. This section describes the criteria used to identify the most appropriate sensor for the smart washer concept.

There are a number of force sensors on the market using a number of operating principles such as the strain gauge, capacitive, piezo-resistive, piezo-electric, non-contact displacement and magneto-elastic sensors[5–10].

These sensors are offered in a variety of technical specifications, form factors and cost. From this list, the piezo-electric, and magneto-elastic were rejected due to the fact that they are better suited to dynamic force measurement; the non-contact displacement sensor was rejected due to the need to deploy more complex sensor electronics and secondary components, such as magnets (Hall effect) and reflectors (optical) respectively; while these candidates offered higher sensitivity and hysteresis, their cost, form factor and power compatibility were unsatisfactory [11]. The advantage and disadvantage in terms of mechanical responses, circuitry complexity and sensor construction for the short listed sensor types, are presented in table 1.

From table 1, it is possible to rank the sensors, having considered each in terms of resolution, accuracy, dynamic range, frequency range, drift and cost. However, the sensor is but one component of the smart washer concept. The choice of sensor will have repercussions in terms of the smart washer design and performance, having an impact on the extent of the sensor processing circuitry, construction of the washer and the integration of these components with an embedded controller as well as communications and power circuits, thus effecting system extent and cost.

To select a force sensing element, the performance of each type has been compared based on the following performance parameters; dynamic range, resolution, frequency range, accuracy, compatibility and robustness. As can be seen in table 2 all of the forces sensing elements show a similar score for performance parameters (21%-24%). In addition to the performance, other parameters such as electronic circuitry, suitability for wireless communication, form factor and construction and sensing element cost were considered to further identify the appropriate sensor.

Table 1. The comparison of short listed force sensor elements.

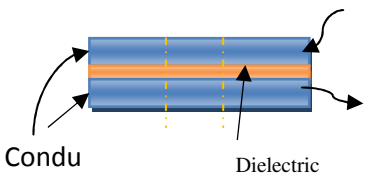

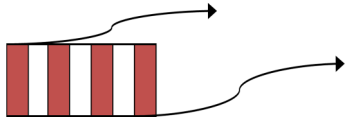
Sensor type	Advantage	Disadvantage
Capacitor [7] 	<ul style="list-style-type: none"> Linear response Cheap sensor element Capability of low frequency (DC) measurement 	<ul style="list-style-type: none"> Complex for circuitry and wireless compatibility High power consumption due to 1 Large circuit area (physical size due to 1 above)
Piezo-resistive (PR1) [8] 	<ul style="list-style-type: none"> Based on resistance measurement Capability of low frequency (DC) measurement Low number of components Capability of static measurement Small circuit area Commercially available 	<ul style="list-style-type: none"> Expensive, FSR unit price ~£9.00 Sensor noise at low loads
Piezo-resistive (PR2) [12] 	<ul style="list-style-type: none"> Based on resistance measurement Capability of low frequency (DC) measurement Low number of components Capability of static measurement Small circuit area 	<ul style="list-style-type: none"> Expensive, FSR unit price ~£1.00 Sensor noise at low loads A prototype sensor

Table 2 also presents a ranking of the clamping force sensor candidates. This ranking shows piezo-resistive sensors to be the preferred choice. This is because the circuitry required to post-process the sensor signal is simple; uses fewer components and consumes less power; the construction is also relatively simple. As can be seen in table 2, there are two piezo-resistive sensors PR1 and PR2; PR1 is the more expensive. Clearly, the cheaper piezo-resistive sensor PR2 receives a higher score than the more expensive piezo-resistive sensor PR1. Having identified the piezo-resistive sensor as most appropriate sensor implementation technology the following sections will consider sensor design, sensor test procedure and an evaluation of performance.

Table 2. Ranking of a smart washer based on the various sensor types.

Sensor type	Performance (25%)	Circuitry (20%)	Cost (20%)	Suitability for wireless (20%)	Construction (15%)	Total (100%)
Capacitive	24	0	20	10	5	59
Strain Gauge	24	10	10	15	5	64
Piezo-resistive (PR1)	22	20	5	20	10	77
Piezo-resistive (PR2)	21	20	20	20	10	91

Note: The higher score the better

3. The design and use of a piezo-resistive sensor

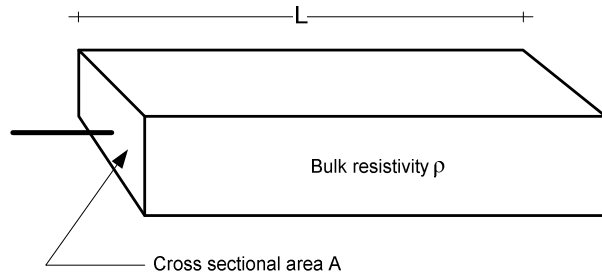
The piezo-resistive effect is described as the change in the electrical resistance of a material due to external stress or material deformation. This effect provides an easy and direct energy/signal transduction mechanism between the mechanical and electrical domains [13]. The resistance of a resistor with length L and cross sectional area A (as shown in Figure 2) is given by:

$$R = \rho \frac{L}{A} \quad (1)$$

By taking the derivative of equation (1); we see that

$$\frac{\Delta R}{R} = \frac{\Delta \rho}{\rho} + \frac{\Delta(L/A)}{L/A} = \frac{\Delta \rho}{\rho} + \left(\frac{\Delta L}{L} - \frac{\Delta A}{A} \right) \quad (2)$$

From equation (2), it can be seen that the resistance of the sample R will change if the area A , length L or bulk resistivity (ρ) is modulated. In practice the piezo-resistive sensor can be considered to be a simple potentiometer.



There are many techniques for measuring such a variable resistance, for example potential divider and Wheatstone bridge arrangements are classic direct current solutions; whereas, resistive control of pulse width modulation (PWM) and frequency of oscillation being common active solutions. The simple passive and active measurement system are shown in figure 3.

Figure 2. Piezo-resistive material mode of operation.

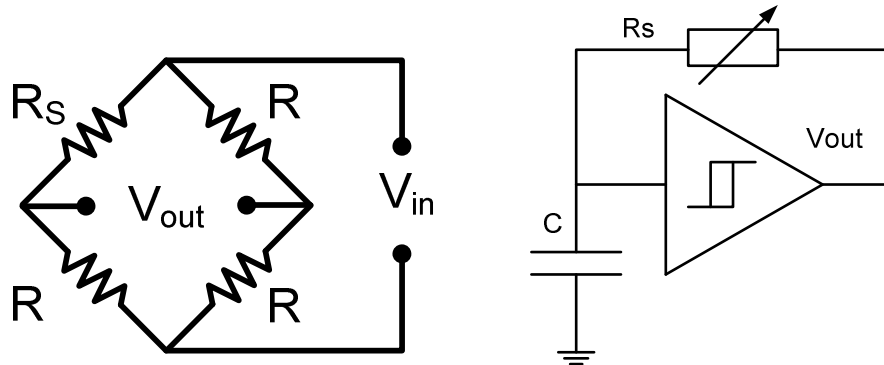


Figure 3. Wheatstone bridge and Schmitt trigger oscillator circuits for dc and ac measurement of varying resistance (R).

Of the two types of circuit presented above, the Wheatstone bridge circuit was adopted due to the simplicity of measurement and the fact that it could be implemented effectively, in terms of cost, size and power requirement. The amplification of the sensor signal is achieved by use of a low power operational amplifier (eg OPA 333) and this presented to a discrete or integrated analogue to digital converter.

3.1 Instrumentation

Having identified the piezo-resistive sensor type as candidate for the smart washer, it was necessary to establish the electrical response of the sensor when subjected to working forces etc. In order to do this it was decided to design an electronic instrumentation circuit which was both satisfactory for laboratory evaluation of the sensor and deployment in the final design. To this end the circuit of Figure 4 was designed and tested.

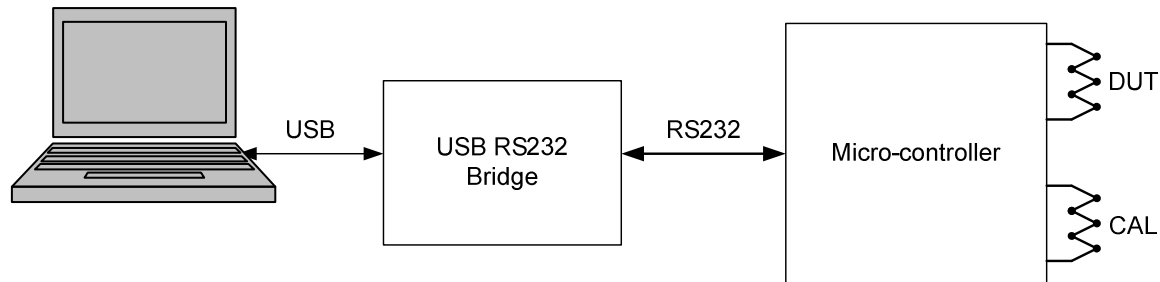


Figure 4. Piezo-resistive sensor instrumentation.

Having tested the circuit of Figure 4 with piezo-resistive sensors PR1 and PR2, it was necessary to consider how the sensors could be tested and evaluated when subjected to a clamping force of 70kN (which is derived from the 250Nm of torque as required specified in the Network Rail maintenance procedures). In order to apply such high clamping force, an experimental rig based around a material testing machine (Instron) and associated instrumentation was developed; indeed the machine was capable of delivering a maximum compressive force of 250kN. The Instron machine was also integrated with axial load and extension test control facility, based on Blue Hill software. The Blue Hill software allows control of the Instron test machine by means of load or extension (compression) single or multiple arbitrary duration cycles. A sketch of the experimental rig is shown Figure 5. Figure 5 shows how the clamping force rig was configured for experiments. It can be seen that the purpose built embedded instrumentation is capable of sampling data from device under test DUT and additional sensors, CAL. The reason for providing additional channels was due to the fact that the Instron machine did not have available an option to acquire data from a third party sensor.

This resulted in difficulties synchronising samples taken by the embedded instrumentation with data sampled by the Blue Hill software respectively. The solution as presented in figure 5 allows the samples originating from the DUT to be temporally correlated with a second sensor measuring either the force exerted (load calibration) or axial displacement (extension calibration).

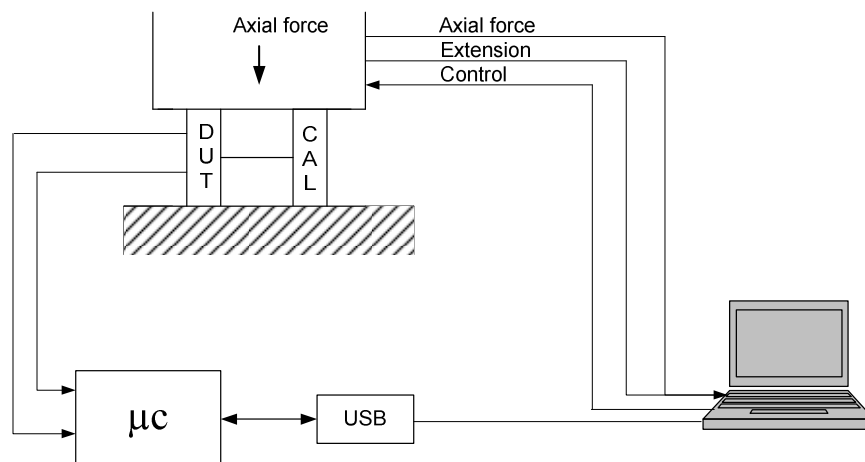


Figure 5. Experimental rig for measuring clamping force.

Another problem concerned the need to test the piezo-resistive sensors up to the specified maximum load of 70kN. It was recognized that applying such a force directly to the sensors, would damage them, as the piezo-resistive material comprising the sensing element would be stressed beyond its' elastic limit. As a consequence it was necessary to consider and implement a means of protecting the sensing element from the directly applied force.

The means for achieving such protection is subject to a patent application; however, the authors are permitted to disclose the fact that the protection is achieved by the use of an elastomer acting as an attenuator of the applied force. Subsequent sections of the paper present the work conducted in order to characterise various elastomers, with the aim of identifying the most appropriate for use in smart washer. Before presenting the results of the elastomer work it is useful to consider the issues associated with deploying a smart washer, particularly the intended form-factor.

3.2 Smart washer form-factor

The majority of bolts used in the rail industry have a threaded diameter of 20mm. After considering the working environment and current structure of rail joint bolts, a smart washer form factor was developed that shown in figure 6 (all dimension are in mm).

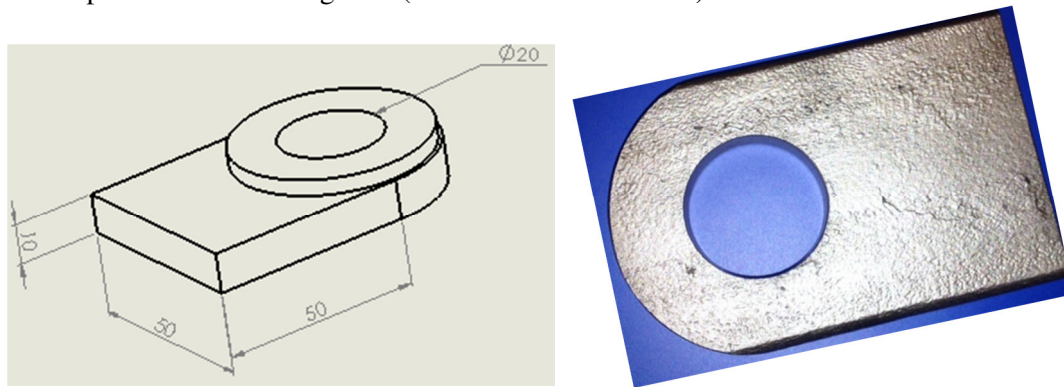


Figure 6. Form factor of smart washer (Design parameters and first generation prototype).

Based on the form-factor, it was decided to conduct all experiments using this form-factor. For intellectual property reasons the actual mechanical arrangement of the washer cannot be published, however the method by which the most appropriate elastomeric attenuator was chosen is presented in subsequent sections. By considering the working environment of the washer, a polymeric material was selected that can resist fluctuations in the environment yet withstand significant loads, applied for long period of time.

4. Sensing element; experimentation and results

The purpose of the smart washer is to provide an electronic measurement of clamping force; however there are two operational issues that must be considered.

1. The specified maximum clamping force is too high to be directly applied to sensor.
2. The sensor must present minimal memory or 'set' to long periods of compression, or conversely, must be able to react to (sense) small changes in clamping force after prolonged periods of compression.

The aim therefore, is to identify a material and means, which in concert with the piezo-resistive element is capable of satisfying these requirements. As stated previously, elastomers were identified as materials that could exhibit the necessary features. To evaluate the behavior of the elastomers, experiments were carried out on the compression and decompression response of the material. Thereafter, the performance of a smart washer using a specific elastomer was determined.

The first experiment was to establish the extension (compression) characteristics of the elastomer. The elastomer was placed in the Instron machine and was subjected to an applied load, compressing the elastomer at a rate of 1mm/min, until the sample was compressed by 2mm; the load was then removed and the elastomer allowed relaxing at the same rate. The periodic extension (compression and relaxation) was repeated twice.

Using this profile it was possible to measure the load bearing capability and response of the elastomer i.e. the force required to compress the elastomer by 2mm and the ability of the sample to return to its' initial (equilibrium) condition. This test is an imitation of tightening a bolt to compress the elastomer by 2mm and the load required to do so and the subsequent slackening of the bolt and observing the ability or otherwise of the elastomer to relax back to a steady (original) state. The experiment was conducted with six elastomer samples of shore hardness 10°, 30°, 40°, 60°, 80° and 90° respectively. Each sample was 5mm in thickness and 40mm in diameter and all were compressed by 2mm. As previously stated the rate of compression and decompression was set at 1mm/min, with each test comprising two cycles. Each sample was tested 3 times.

4.1 Preliminary elastomer investigation

Using the procedure of section 4, the first activity was to understand the difference in response as function of the Shore hardness of the elastomer (60° means a shore hardness of 60). Six samples of silicon elastomer of varying shore hardness (10°, 30°, 40°, 60°, 80°, 90°) were each subjected to the extension control profile, to establish their load response verses extension for one full cycle, figure 7.

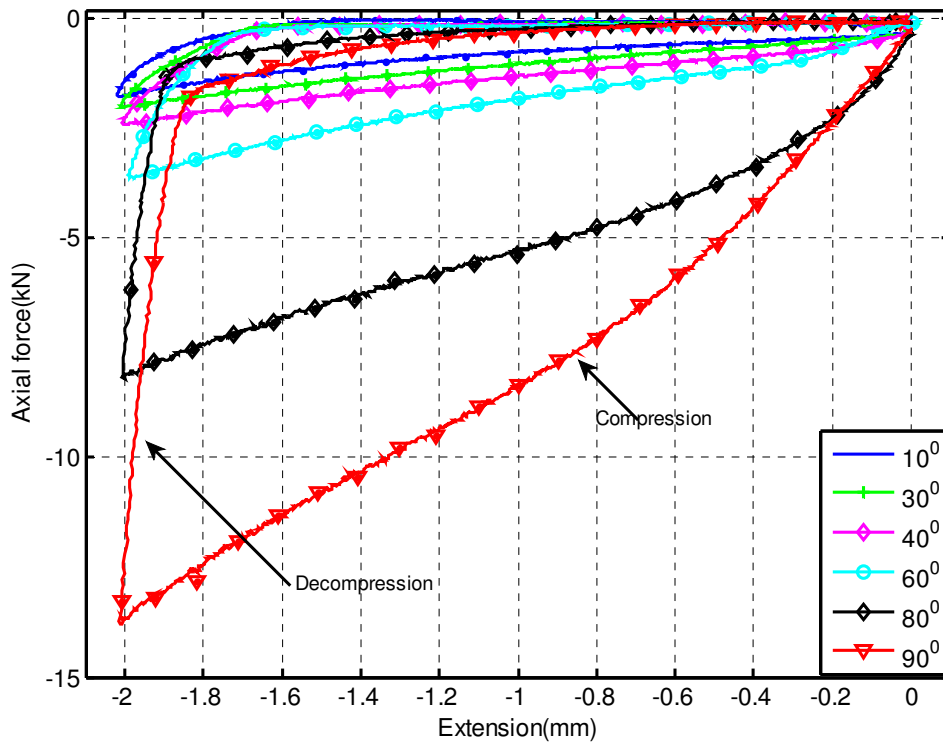


Figure 7. Axial force response verses extension for one full cycle for range of elastomer.

During compression, the cross-linked nature of the elastomer ensures that permanent chain slippage is largely avoided during deformation and hence all of the elastomers return to their original location upon release of the strain; i.e. they exhibit elastic behaviour [14]. It can be seen from figure 7 that the compression phase is relatively linear with applied load. In this test, the Instron testing machine was configured to use extension as the control parameter;

hence the load was varied to achieve the desired compression. However, during the relaxation phase, the response was very different. Initially there was a rapid change in force for a small change in extension (-2.0mm to -1.8mm for 90°). Thereafter, the elastomer recovered to zero over the range -1.8mm to 0mm. Thus, the decompression may be regarded as a piece-wise linear approximation with two responses either side of a transition point.

The two piece-wise linear components of the relaxation phase of the cyclic tests of the load vs. extension graphs of figure 7 are worthy of closer scrutiny. It is interesting to consider the gradient of the load (applied force AF) vs. extension curve for the relaxation process only.

From figure 7 we note that each relaxation curve undergoes a change in gradient once as it is extended beyond -1.75mm. After this point the gradient changes significantly. In order to further scrutinize the change in gradient, each of the Shore hardness traces in figure 7 were subject to curve fitting, and their derivative plotted against extension; figure 8. The piecewise linear nature of the rate of change of load with extension is clear in figure 8.

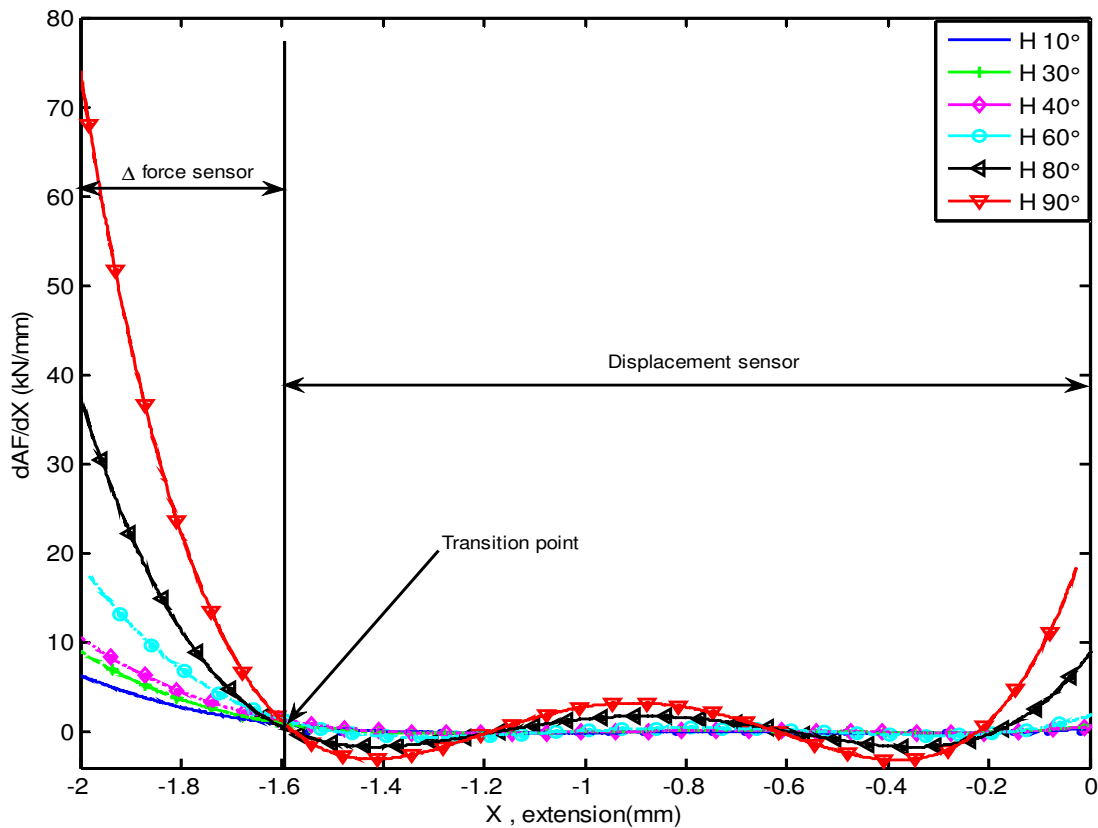


Figure 8. Modes of sensing available when using an elastomer.

From the responses shown in figure 8 two distinct methods for using the elastomer in a sensing system are observed.

- Displacement sensor: over the range 0 to -1.75mm, the sensor will record small changes in force for changes in compress thickness $0 > x > -1.75$ mm
- Differential force sensor:- over the range -1.75mm to -2.0mm, the sensor provides significant load changes for small changes in x , i.e. when $-1.75 > x > -2.0$ mm.

To investigate the relationship between the load response and the shore hardness of the elastomer, a measurement of the load required to compress a sample of specific Shore hardness by 2mm was taken; the results for a number of samples of various Shore hardness is

shown in figure 9. It can be seen that when the Shore hardness increases, the load required to compress the elastomer by the specified 2mm, also increases.

The relation between the hardness (H) and axial force (AF) is fitted with a second regression polynomial equation (3) with R equal to 98% for cycle 1. This relationship can be used to assist the selection of an elastomer with the appropriate Shore hardness for use in the smart washer design based on the maximum attainable axial load distribution and the structural arrangement.

$$AF = -0.0025H^2 + 0.136H - 3.3760 \quad (3)$$

To investigate the effect of hardness on the hysteresis of the elastomer, an experiment was conducted which subjected samples of various shore hardness to five consecutive cycles as shown in Figure 9.

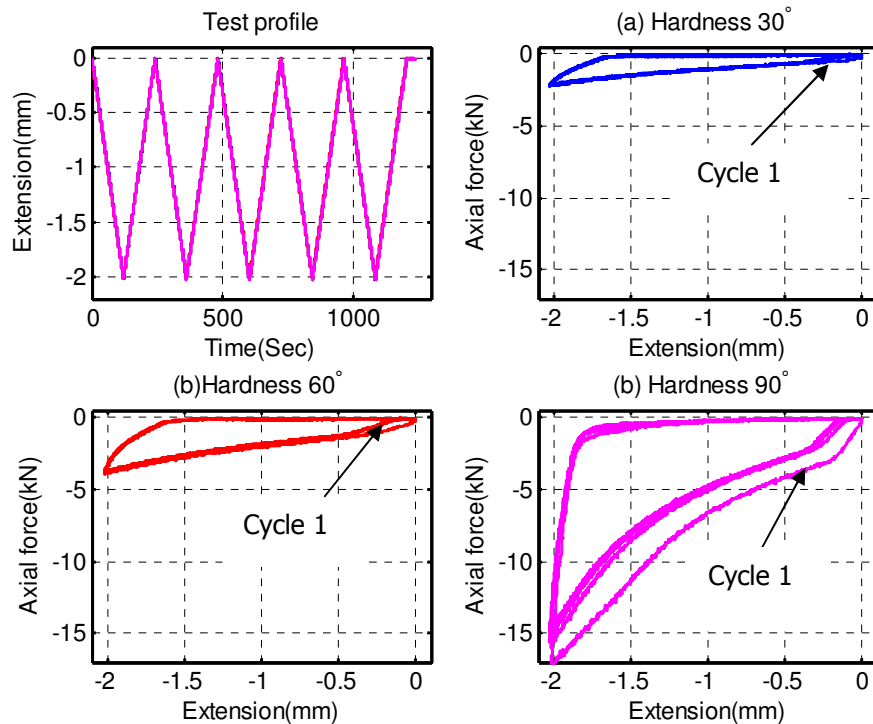


Figure 9. Axial force vs extension responses for hardness of 30°, 60° and 90° Shore.

The load versus extension curves for samples of Shore hardness of 30°, 60° and 90° are shown in figure 9(b-d). It can be seen that when the shore hardness increase hysteresis of the elastomer also increases slightly. As would be expected, the hysteresis curves are consistent apart from the first cycle, cycle 1, which is unique and never again repeated, as per the Mullins Effect [15]. This hysteresis curves or more specifically the recoil response, will be used to select the most appropriate elastomer for use in the smart washer.

So far the results presented were collected from samples of a high-quality, industrial grade elastomer, of varying Shore hardness. The authors were keen to investigate the comparative performance of cheaper commercial grade elastomers; this analysis is now presented. In order to distinguish between the two silicon types the industrial silicon elastomer described in previous sections will be designated silicon industrial grade SIG, with the cheaper commercial grade silicon designated silicon commercial grade SCG.

The force extension graphs for SIG and SCG samples of 40° and 60° Shore are shown in Figure 10. In figure 10 the blue and red traces relate to industrial grade and commercial grade silicon elastomers respectively. In addition the solid and dashed lines refer to 40° and 60° Shore samples respectively. As can be seen in Figure 10, the commercial grade silicon of 60° Shore hardness withstands highest compressive load. This will be due to the chemical composition of the grades.

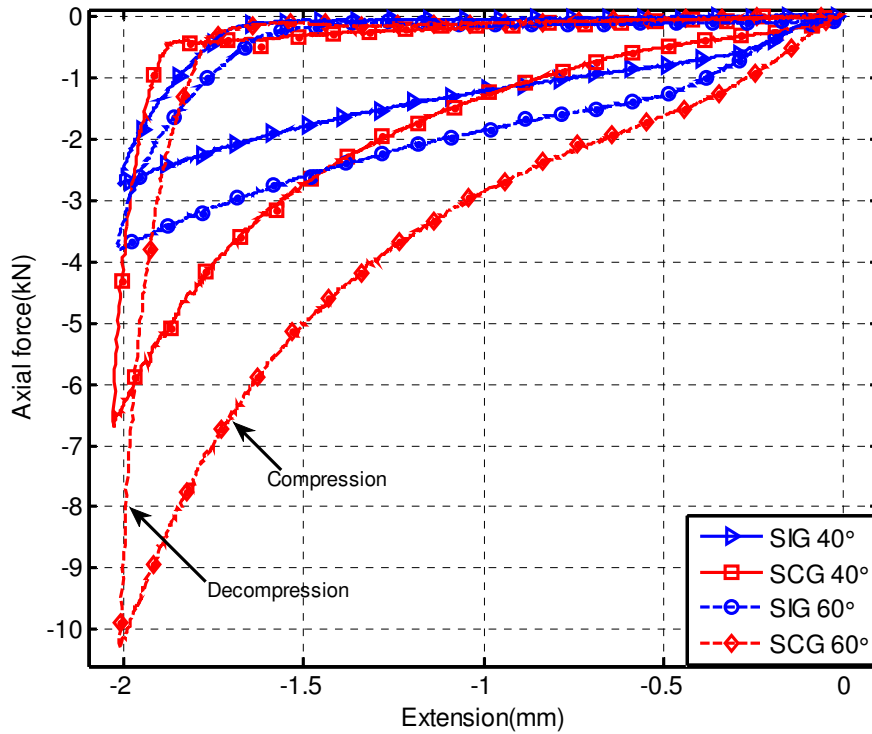


Figure 10. Comparison of the force extension response for SIG and SCG elastomers.

5. Smart washer design and performance

From figure 10 we see that the cheaper commercial grade silicon SCG with a Shore hardness of 60, supports a greater load for a nominal compression of 2mm when compared to commercial grade silicon of a lower shore hardness any of the industrial grade silicon. Specifically this sample provides the greatest change in load (recovery or recoil force) over the smallest change in extension. This ensures that, in the absence of any permanent “set” in the material, the 60° SCG will respond with the greatest change in load force for displacement changes of <0.2mm.

In practice, a 20mm bolt, as used in rail industry has a thread pitch of 2mm. Therefore, a sensor based on 60° SCG will provide the greatest change in axial force over 0.2/2 of a turn of the nut or bolt, i.e. 36°. However, while the elastomer is capable of controlling the applied force to the sensor by means of viscous elasticity, the maximum applied load in use is still too high for the elastomer and sensor to bear. Attenuation of the maximum applied force is therefore necessary and is achieved by a novel compound spring damper arrangement. The authors are not at liberty to disclose the details of this arrangement, however they have permission to disclose the test method and report the results and conclusions drawn there-from.

Two variants of the washer design were constructed and tested; these were termed HUS1 and HUS2 respectively. The variants were tested in two ways.

1. Each variant was subject to a compression test allowing the strain as a function of applied load (to a maximum of 70kN) to be determined. In addition, the change in resistance of the sensing element, as a function of the applied load was also measured during the test using an Ohm meter.
2. Each variant was subject to a compression test allowing the strain as a function of applied load (to a maximum of 70kN) to be determined; but rather than measure the resistance of the sensor directly, the instrumentation described in section 3.1 was used.

Hence the voltage measured across the piezo-resistive sensor element was sampled by an analogue to digital (A/D) convertor the output of which was sent to and stored on a personal computer.

Figure 11 and Figure 12 show plots of the strain verses the applied axial load applied for washer designs HUS1 and HUS2 respectively. As can be seen from Figure 11(a) and Figure 12(a), the applied axial force and the strain are strictly nonlinear, however the extent of the nonlinearity appeared to be small and hence a linear approximation was fitted to the data to assess a nominal degree of error. The error between the measured and predicted data for the HUS1 and HUS2 designs are shown in Figure 11(b) and Figure 12(b) respectively.

A first degree regression correlation between the axial force (AF) and strain ($\Delta L/L$) were developed for HUS1 with R^2 values of 0.984 and 0.975 for compression and decompression respectively.

$$\varepsilon_{c1} = 3.9AF/1000 + 0.0283 \quad (4)$$

$$\varepsilon_{dc1} = 3.6AF/1000 + 0.0654 \quad (5)$$

Where ε_{c1} is the strain for compression with HUS1 and ε_{dc1} is the strain for decompression with HUS1.

Similarly, a first degree regression correlation between the axial force (AF) and strain ($\Delta L/L$) were developed for HUS2 with R^2 values of 0.994 and 0.985 for compression and decompression respectively.

$$\varepsilon_{c2} = 1.9F/1000 + 0.0498 \quad (6)$$

$$\varepsilon_{c2} = 1.7F/1000 + 0.0719 \quad (7)$$

Where ε_{c2} is the strain for compression with HUS1 and ε_{dc2} is the strain for decompression with HUS2.

As previously stated, the change in resistance, (as measured using an Ohm-meter), due to the applied axial load (clamping force) and as a function of strain ($\Delta L/L$) for spring washer designs HUS1 and HUS2 was recorded. Figure 13 shows the normalized change in resistance ($k\Omega$) for each washer design as a function of axial force and strain.

It can be seen from figure 13 that the change in the electrical resistance of both smart washer designs, decreases with an applied axial compression force and reversibly increases when the load is removed. The relationships between the resistance change and the axial load for both designs is non-linear.

The graphs of normalize resistance vs. axial force appear to be second order; to confirm this, the data was subject to curve fitting. The curve fitting was achieved by performing a regression analysis using the actual resistance values, for both compression and decompression. The results of the regression analysis are presented in table 3.

Table 3. Regression equation and R^2 values.

Process and spring	Regression equation	R^2 value
Compression : HUS1	$\Delta R = 0.0005AF^2 - 0.063AF + 1.877$	0.990
	$\Delta R = 26.72\varepsilon^2 - 14.75\varepsilon + 2.305$	0.985
Decompression : HUS1	$\Delta R = 0.005AF^2 - 0.0583AF + 1.712$	0.976
	$\Delta R = 15.68\varepsilon^2 - 11.72\varepsilon + 2.30$	0.967
Compression : HUS2	$\Delta R = 0.0004AF^2 - 0.043AF - 3.827$	0.982
	$\Delta R = 76.97\varepsilon^2 - 25.07\varepsilon + 2.26$	0.978
Decompression : HUS2	$\Delta R = 0.0003AF^2 - 0.0376AF - 3.668$	0.967
	$\Delta R = -41.85\varepsilon^2 - 1.96\varepsilon + 1.675$	0.967

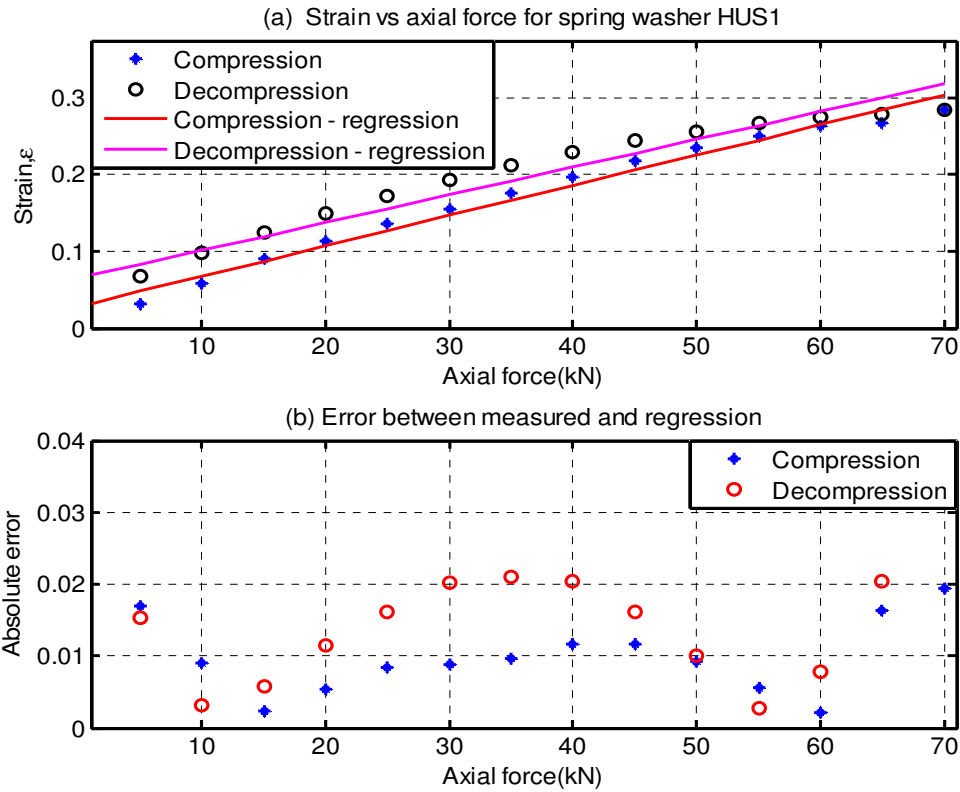


Figure 11 Load extension profile of the smart washer design HUS1

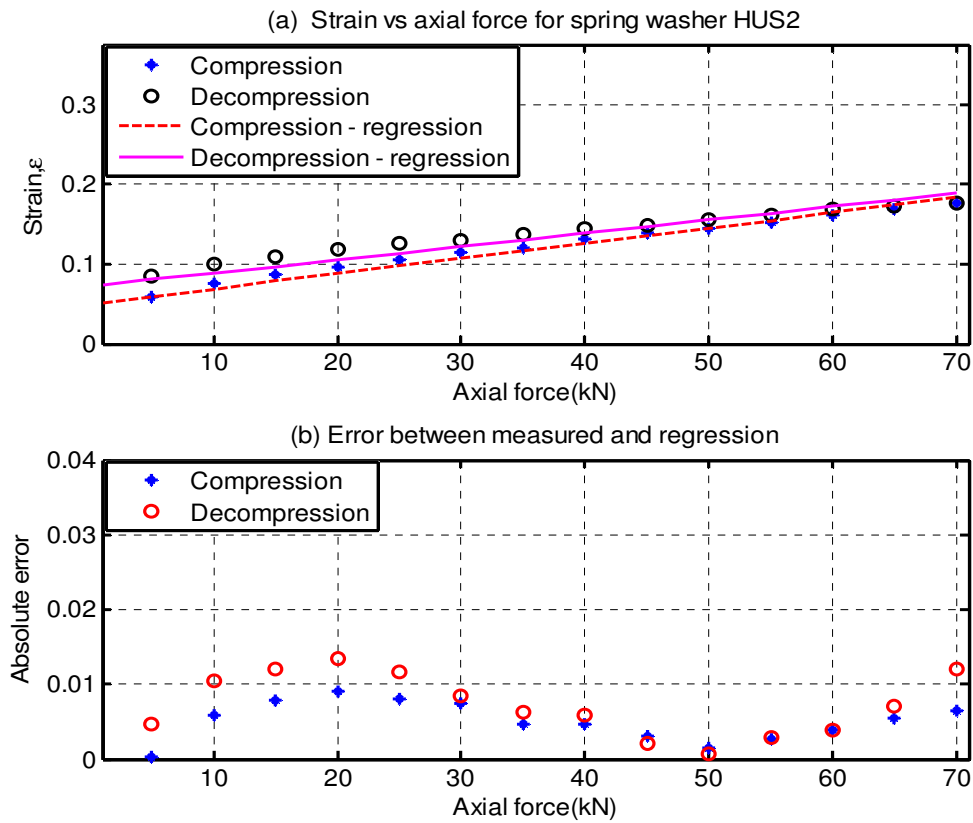


Figure 12. Load extension profile of the smart washer design HUS2.

HUS1 expresses a good second order response, repeatable in both compression and decompression. HUS2 shows a comparable second order decompression behavior to HUS1 however it also shows a hysteresis with the compression phase. This hysteresis is due to the choice of material used in the design of HUS2. Mathematical approximations of the response curves for HUS1 and HUS2 in states of compression and de-compression have been calculated, table 3. In table 3, AF is the axial force, ΔR is change of resistance, ε is the strain and R^2 is the square coefficient value.

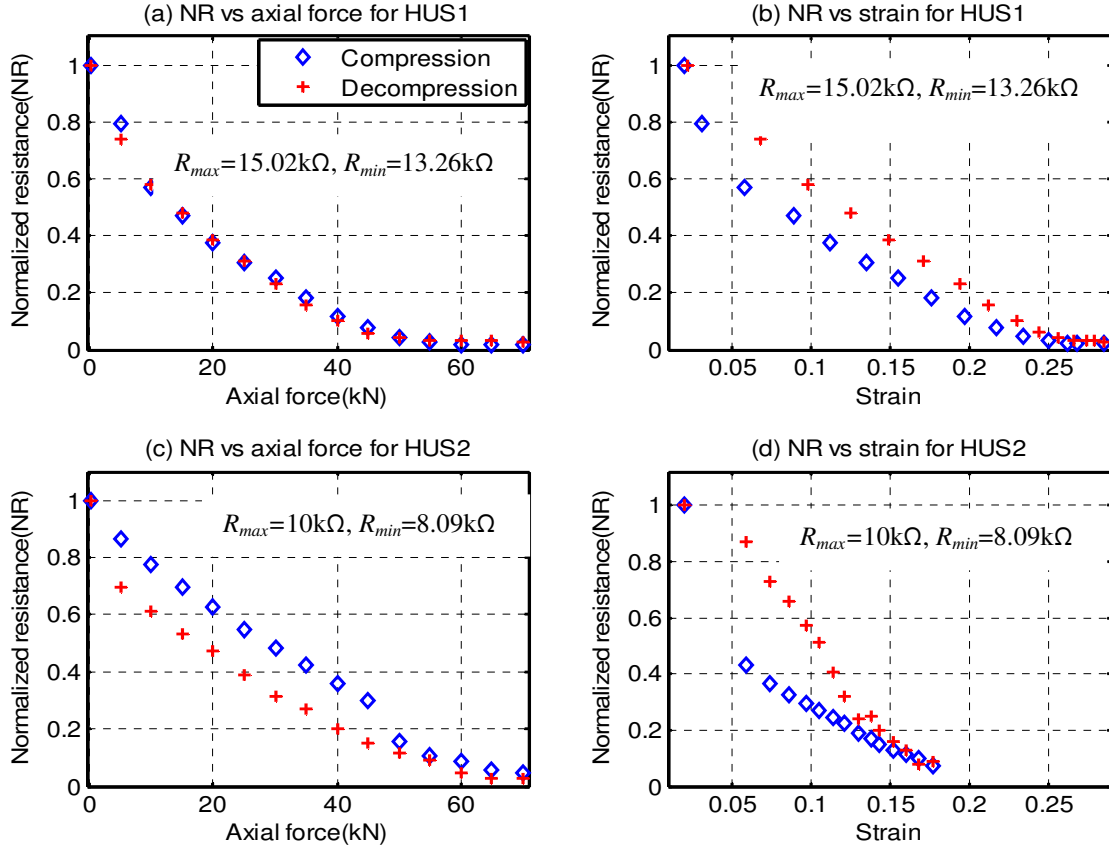


Figure 13. Normalized resistance versus axial force and strain.

The presence of hysteresis in the response curve of HUS2 means that it is unsatisfactory for the measurement of applied load however the sensor design of HUS2 could be used to detect relative changes in applied load. The repeatable nature of the HUS1 design means that it is the most appropriate design for measuring applied load.

Given the (repeatable) second order response of the resistance vs load curve of HSU1, matter to linearise the response using the micro-controller based instrumentation described in section 3.1. Washer design HUS1 was subject to a load bearing test over the range 0 to 70kN with the response of the washer in terms of an eight bit digital value being recorded. Figure 14 shows, the normalized digital output of the system vs the axial load, for compression and decompression states. It can be seen that the output of the HUS1 sensor is linear over the higher ranges of applied force, as required by the design. Indeed the result is very linear in the decompression phase, which is important for this is the phase of interest as the tensile force of the bolt reduces due to slackening. The comparatively non-linear behavior of the sensor in compression (i.e during tightening) and the fact that the compression and decompression curves diverge at higher levels of applied force are the subject of ongoing work.

The results of section 5 show that the smart washer design HUS1 is capable of utilizing a combination of fragile piezo-resistive sensor, elastomer and intelligent design to measure the

extremely high clamping force associated with bolted joints, as found on railway infrastructures and furniture, such as points.

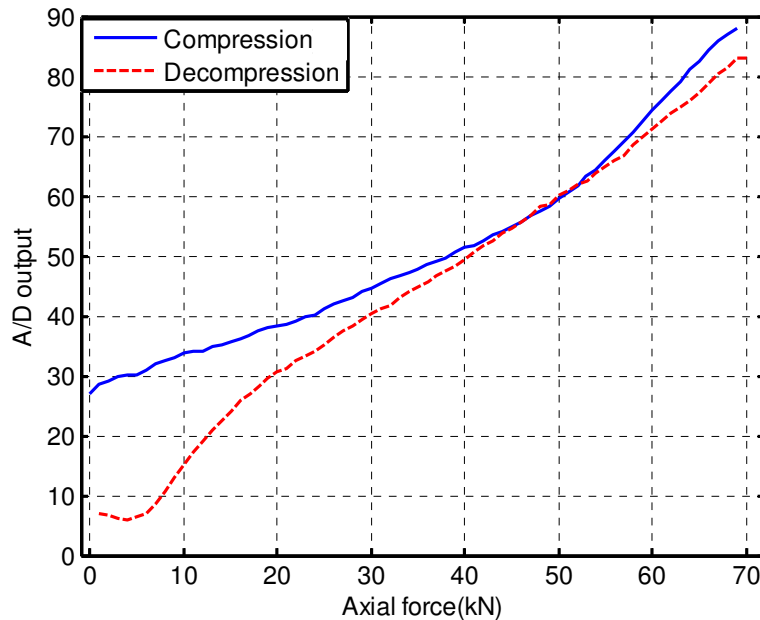


Figure 14. The digital response curve of the washer design HUS1 as a function of applied axial force.

6. Conclusion

In this study a piezo-resistive based clamping force sensor, packaged as a smart washer, has been developed by using a combination of fragile piezo-resistive sensor elements, elastomers and other components. The response of the smart washer has been measured for a range of applied axial load. The resulting change in resistivity of the sensor has shown non-linear relationship with the axial load. Using experimentation and analysis methods a system comprising an embedded electronic circuit was developed to produce a linear digital output measure of applied axial load over the range 20 to 70 kN. The results show that the smart washer has the potential to monitor the clamping force of bolted joints, in-situ, as found on the stretcher bars present in all railway points. The results are encouraging and support development of the other components needed to integrate the smart washer sensor into the communications network necessary for automatic distribution of clamping force data.

Acknowledgements

The authors recognise the support of Smart Components Ltd., Network Rail and Yorkshire Forward.

Reference

- [1] Network Rail UK Railway Statistics [Online]. Available: <http://www.railway-technical.com/statistics.shtml> [Accessed: 31-Jan-2012]
- [2] RAIB Rail Accident Investigation: 071003_IR022007_Grayrigg [Online] Available: http://www.raib.gov.uk/publications/interim_reports/071003_ir022007_grayrigg.cfm . [Accessed: 11-Mar-2012]
- [3] Minguez J M and Vogwell J 2005 Theoretical analysis of preloaded bolted joints subjected to cyclic loading *International Journal of Mechanical Engineering Education*, **33** 4 349-357
- [4] SKF Group 2001 Bolt-tightening Handbook 1st ed France

- [5] Elbestawi M A 1999 The Measurement, Instrumentation and Sensors Handbook on CD-ROM Crc Press Llc
- [6] Kalantari M, Ramezanifard M, Ahmadi R, Dargah J and Kovecses J 2010 Design, fabrication, and testing of a piezoresistive hardness sensor in Minimally Invasive Surgery *IEEE Haptics Symposium* 431-437
- [7] Arshak K I, McDonagh D, and Durcan M A 2000 Development of new capacitive strain sensors based on thick film polymer and cermet technologies *Sensors and Actuators A: Physical* **79** 2 102-114
- [8] FlexiForce, FlexiForce Force Sensors A Force Sensor with a Single Button Force Sensing Resistor [Online]. Available: <http://www.tekscan.com/flexible-force-sensors>. [Accessed: 31-Jan-2012]
- [9] Kon S, Oldham K and Horowitz R 2007 Piezoresistive and Piezoelectric MEMS Strain Sensors for Vibration Detection *Sensors and Smart Structures Technologies for Civil, Mechanical, and Aerospace Systems Proc. of SPIE Vol. 6529 65292V-1*
- [10] Falk L T 2008 Strain gauge based microsensor for stress analysis in building structures *Measurement* **41** 10 1144-1151
- [11] Shieh J, Huber J, Fleck N, and Ashby M 2001 The selection of sensors, *Progress in Materials Science* **46**, 3-4461-504
- [12] Huang C T, Shen C L, Tang C F and Chang S H 2008 A wearable yarn-based piezoresistive sensor *Sensors and Actuators A: Physical* **141** 2 396-403
- [13] Johns G K 2006 *J App Engineering Mathematics* **2** 2006
- [14] Ayca E and Narasi S 2009 performance of elastomeric materials in gasoline - ethanol blends -a review *NACE International CORROSION 2009 Annual Conference and Exhibition Atlanta 2009*
- [15] Mullins and Tobin N R 1965 Stress softening in rubber vulcanizes. Part I. Use of a strain amplification factor to describe the elastic behaviour of filler-reinforced vulcanized rubber *J. App. Polymer Science* **9** 9 2993-3009